JACS
JOURNAL OF THE AMERICAN CHEMICAL SOCIETY

Article

pubs.acs.org/JACS

Potentiometric Titrations for Measuring the Capacitance of Colloidal Photodoped ZnO Nanocrystals

Carl K. Brozek, Kimberly H. Hartstein, and Daniel R. Gamelin*

Department of Chemistry, University of Washington, Seattle, Washington 98195-1700, United States

Supporting Information

ABSTRACT: Colloidal semiconductor nanocrystals offer a unique opportunity to bridge molecular and bulk semiconductor redox phenomena. Here, potentiometric titration is demonstrated as a method for quantifying the Fermi levels and charging potentials of free-standing colloidal *n*-type ZnO nanocrystals possessing between 0 and 20 conduction-band electrons per nanocrystal, corresponding to carrier densities between 0 and 1.2×10^{20} cm^{-3}. Potentiometric titration of colloidal semiconductor nanocrystals has not been described previously, and little precedent exists for analogous potentiometric titration of any soluble reductants involving so many electrons. Linear changes in Fermi level vs charge-carrier density are observed for each ensemble of nanocrystals, with slopes that depend on the nanocrystal size. Analysis indicates that the ensemble nanocrystal capacitance is governed by classical surface electrical double layers, showing no evidence of quantum contributions. Systematic shifts in the Fermi level are also observed with specific changes in the identity of the charge-compensating countercation. As a simple and contactless alternative to more common thin-film-based voltammetric techniques, potentiometric titration offers a powerful new approach for quantifying the redox properties of colloidal semiconductor nanocrystals.

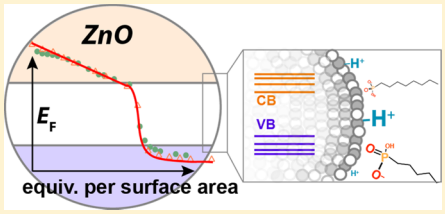

INTRODUCTION

Quantum dot solar cells,[1] light-emitting diodes (QLEDs),[2] photodetectors,[3] and photocatalysts[4−6] all rely at a fundamental level on electron transfer across semiconductor-dielectric interfaces at the nanocrystal surfaces. Tailoring nanocrystals for a given application requires knowledge of their redox potentials, which determine band offsets at junctions in quantum-dot devices and affect numerous phenomena such as internanocrystal electron-transfer rates in colloids or variable-range hopping in quantum-dot solids. In colloidal applications such as solar-fuels generation, nanocrystal redox potentials impact electron-transfer and proton-coupled electron-transfer reaction driving forces.[7] The charging and discharging of colloidal semiconductor nanocrystals is fundamentally intriguing because it resembles both molecular redox reactivity and the interfacial electron-transfer properties of bulk semiconductor-liquid junctions. Reliable measurement of the redox potentials of free-standing colloidal nanocrystals has posed long-standing challenges, however. Surface chemistry is known to influence the band-edge potentials of semiconductor nanocrystals through surface-dipole and electrostatic effects,[8] but the surfaces of such nanocrystals as free-standing colloids are dynamic and hence extremely complicated. For many nanocrystals, voltammetric measurements display irreversible waves, complicating interpretation further. Additionally, voltammetric techniques are intrinsically nonequilibrium methods involving current flow at applied bias. Recently, we reported the use of potentiometry as a nondestructive method to measure the Fermi levels (E_F) of colloidal semiconductor nanocrystals during photochemical accumulation of conduction-band electrons (e^-_{CB}).[9] Here, we demonstrate potentiometric titration as a powerful method for quantifying e^-_{CB} potentials over a broad range of equilibrium carrier densities in colloidal nanocrystals. This method allows facile interpretation of the measured potentials in terms of nanocrystal capacitance and provides quantitative insight into the microscopic factors that affect the nanocrystal redox properties.

Photodoping is among the most thoroughly investigated and most convenient strategies for electronic doping of colloidal semiconductor nanocrystals.[10−14] Upon nanocrystal photoexcitation, an electron from the valence band (VB) is promoted to the conduction band (CB). The photogenerated hole can be rapidly quenched in the presence of a sacrificial donor such as EtOH or $Li[HBEt_3]$. When using EtOH as the reductant, acetaldehyde is generated as the oxidation product, with liberated H^+ balancing the e^-_{CB} charge. This photochemical process allows accumulation of multiple e^-_{CB} per ZnO nanocrystal, and these electrons are stable indefinitely under rigorously anaerobic conditions. With the average number of e^-_{CB} per nanocrystal ($\langle n \rangle$) exceeding 100 in certain cases,[14] corresponding to maximum carrier densities as large as $\langle N \rangle \approx 6 \times 10^{20}$ cm^{-3} depending on the reductant, photodoped ZnO nanocrystals offer unique opportunities to study the fundamental properties of excess charge carriers in colloidal semiconductor nanocrystals.

EXPERIMENTAL SECTION

General Considerations. Unless stated otherwise, all measurements and synthetic manipulations were performed with standard

Received: June 7, 2016
Published: July 22, 2016

ACS Publications © 2016 American Chemical Society

DOI: 10.1021/jacs.6b05848
J. Am. Chem. Soc. 2016, 138, 10605−10610

Schlenk techniques under a dinitrogen atmosphere, or in a glovebox under an atmosphere of purified dinitrogen. Anhydrous tetrahydrofuran (THF) was purified through an alumina column pressurized with Ar.

Chemicals. Zinc acetate dihydrate ($Zn(OAc)_2{\cdot}2H_2O$, >98%), tetramethylammonium hydroxide pentahydrate (TMAH, > 97%), dodecylamine (DDA, 98%), 1,8-bis(dimethylamino)naphthalene, (Proton Sponge, 99%), bis(cyclopentadienyl)cobalt(III) hexafluorophosphate ($[CoCp_2][PF_6]$, 98%), and trioctylphosphine oxide (TOPO, 90%) were purchased from Sigma-Aldrich and used without further purification. Anhydrous EtOH was obtained from Acros and stored under dinitrogen in a glovebox. (2,2,6,6-Tetramethylpiperidin-1-yl)oxyl ("TEMPO", 99%, Sigma-Aldrich) was purified through sublimation, and tetrabutylammonium hexafluorophosphate ($TBAPF_6$, 98%, Sigma-Aldrich) was recrystallized prior to use. Decamethylferrocenium tetrakis[3,5-bis(trifluoromethyl)phenyl]borate ($[Fc^*][BAr^F{}_4]$) was prepared according to a literature procedure.[15] For this purpose, $FeCl_3$ (99.9%), bis(pentamethylcyclopentadienyl)iron(II), and sodium tetrakis[3,5-bis(trifluoromethyl)phenyl]borate were bought from Sigma-Aldrich and used without further purification.

Nanocrystal Synthesis. ZnO nanocrystals were synthesized by base-initiated hydrolysis and Zn^{2+} condensation according to previously reported methods.[16,17] In a typical synthesis, 22 mmol of TMAH were dissolved in 40 mL of ethanol EtOH and added dropwise to a stirring solution of 13 mmol of $Zn(OAc)_2{\cdot}2H_2O$ in 135 mL of dimethyl sulfoxide (DMSO) at room temperature. For smaller ZnO nanocrystals, $Zn(OAc)_2{\cdot}2H_2O$ was instead dissolved in 2:1 DMSO/EtOH and stirred on ice during dropwise addition. The reaction was quenched immediately with addition of excess ethyl acetate. Pellets were collected by centrifugation, resuspended in EtOH, and reprecipitated with addition of hexanes and centrifugation. Surface ligands were exchanged by heating the pellets in excess DDA (10−30 min, depending on desired size) and precipitation with EtOH. The pellets were subsequently heated in excess TOPO (10−30 min) and washed with alternating cycles of suspension in hexanes and precipitation with EtOH, before final suspension in toluene or THF for further measurements and characterization.

Nanocrystal Photodoping. ZnO nanocrystals (6 μM) were suspended in a THF solution containing $TBAPF_6$ as the supporting electrolyte and ethanol as the hole-quencher, according to previous reports.[11,13,14] These were then photodoped by illumination with a 340 nm photodiode (10 mW).

Determination of $\langle n \rangle$. The average number of excess conduction-band electrons per photodoped ZnO nanocrystal ($\langle n \rangle$) was determined by titration using $[Fc^*][BAr^F{}_4]$ as the titrant.[14,18] Aliquots of $[Fc^*{}_2][BAr^F{}_4]$ in THF were added to photodoped ZnO nanocrystals, and the mixtures were monitored by optical spectroscopy until the NIR absorption feature was eliminated. The total number of ZnO CB electrons introduced by photodoping was then calculated as the x-intercept of these data and converted to $\langle n \rangle$ using the analytical ZnO nanocrystal concentration as determined by inductively coupled plasma atomic emission spectroscopy (ICP-AES).

Potentiometry. Measurements were conducted using a customized three-electrode electrochemical cell (Figure S1) kept inside a dinitrogen-filled glovebox. The cell comprised a septum-capped quartz cuvette containing two platinum wires as the working and counter electrodes and a 1 mm Ag/AgCl leakless reference electrode (Edaq). Open-circuit potentials were recorded using a Gamry potentiostat under galvanostatic control at $I = 0$ A. Reactions were considered to be at Nernstian equilibrium once they stabilized to a variation below 0.05 mV per second. Potentials vs Fc^+/Fc were determined by collecting cyclic voltammograms on the solutions at the end of potentiometric experiments using additional $[CoCp_2][PF_6]$ as an internal standard.

Physical Characterization. Nanocrystals were dried under vacuum, then dispersed in anhydrous THF, and stored in a dinitrogen glovebox. UV−vis−NIR spectra were measured using a Varian Cary 5000 spectrophotometer. Nanocrystal radii for all samples were determined through the Scherrer relation by power X-ray diffraction collected using a Bruker D8 Discover. Average sizes and size distributions were also estimated by spectroscopic analysis of the first excitonic absorption following literature methods.[19,20] For the largest nanocrystals, the standard deviation on the mean was assumed to be the same as those found for the other sizes (~16%). Zn concentrations of the nanocrystal solutions were measured by ICP-AES with a PerkinElmer Optima 8300 spectrophotometer.

RESULTS AND ANALYSIS

Scheme 1 summarizes the reactions employed in this study. Colloidal ZnO nanocrystals were maximally photodoped by

Scheme 1

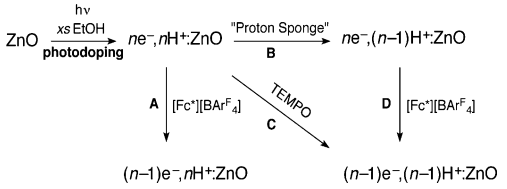

340 nm irradiation of air-free suspensions containing excess EtOH, forming ne^-,nH^+:ZnO. Subsequently, various titrants were added to the photodoped nanocrystal suspensions to probe their effect on the nanocrystal Fermi level. Pathways A−D indicate the specific titrations that were performed (see Supporting Information for details).

Figure 1A plots the open-circuit potential (V_{OC}) measured for a ne^-,nH^+:ZnO suspension vs the number of oxidizing equivalents added in the form of decamethylferrocenium tetrakis[3,5-bis(trifluoromethyl)-phenyl]borate ($[Fc^*][BAr^F{}_4]$, pathway A). V_{OC} shifts monotonically toward more positive potentials, with a linear slope of +32.8 mV/eqiuv. When the number of oxidizing equivalents added to the suspension equals the average maximum number of e^-_{CB} per nanocrystal ($\langle n \rangle$) deposited by photodoping, V_{OC} drops suddenly toward the formal potential ($E^{o\prime}$) of the titrant, thus producing a sigmoidal curve that is characteristic of potentiometric titrations. Because V_{OC} reflects E_F of the entire solution, the slope in the titration curve indicates that the nanocrystals are stabilized by 32.8 mV per e^-_{CB} across the entire range of electron densities. In this titration, the number of H^+ associated with the nanocrystals remains fixed at the value introduced through photodoping. This measurement also provides E_F at chemical equilibrium for different values of $\langle n \rangle$ within the ensemble of ZnO nanocrystals.

In addition to titrating electrons at fixed values of H^+ per nanocrystal, we performed measurements on the same nanocrystals using a Brønsted base to titrate H^+ (pathway B) at a fixed value of $\langle n \rangle = \langle n \rangle_{max} \approx 10$. Here, the number of excess H^+ per nanocrystal decreases from n_{max} to $n_{max} - m$ in proportion to the amount of added base. As shown in Figure 1B, V_{OC} grows increasingly negative with addition of 1,8-bis(dimethylamino)naphthalene, "Proton Sponge". The titration appears to be complete after only ~8 equiv of base. This result suggests that only the number of H^+ generated via photodoping are removable by this base, and not additional H^+, e.g., present from the initial nanocrystal synthesis. Subsequent titration of the electrons using $[Fc^*][BAr^F{}_4]$ (Figure S4, pathway D) yields the same number of electrons per nanocrystal as Proton Sponge equivalents needed to reach the titration end point in Figure 1B (~8), indicating that approximately 10% of the e^-_{CB} were lost in the process of adding 10 equiv of base and no oxidant (Figure S3). Perhaps removal of multiple H^+ per nanocrystal makes the remaining

DOI: 10.1021/jacs.6b05848
J. Am. Chem. Soc. 2016, 138, 10605−10610

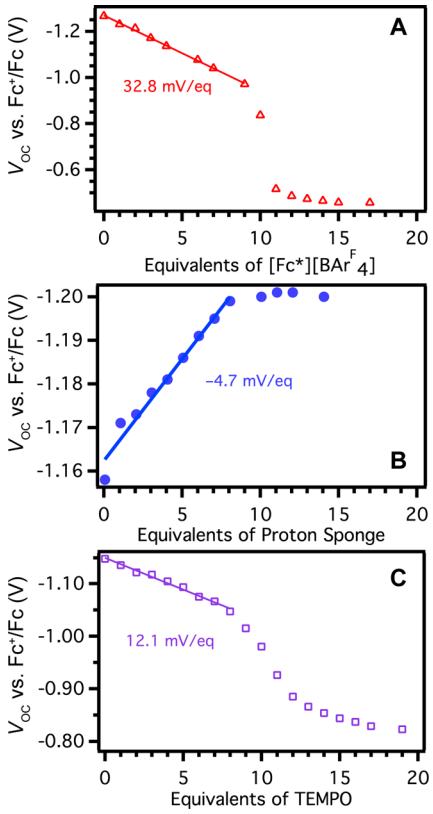

Figure 1. Potentiometric titrations of maximally photodoped colloidal d = 6.1 nm ZnO nanocrystals. Open-circuit potentials (V_{OC}) are plotted against equivalents of added titrant, which were as follows: (A) [Fc*][BAr^F_4], (B) 1,8-bis(dimethylamino)naphthalene ("Proton Sponge"), and (C) (2,2,6,6-tetramethylpiperidin-1-yl)oxyl ("TEMPO"). Slopes derived from linear fits are included in each panel. Measurements were performed using 6 μM ZnO nanocrystals in THF solutions containing 0.1 M tetrabutylammonium hexafluorophosphate ($TBAPF_6$).

e^-_{CB} sufficiently reactive to reduce other H^+, or perhaps some e^-_{CB} are simply lost during the experimental manipulations. Regardless, these data demonstrate that the ZnO nanocrystals are rendered substantially more reducing by removing H^+ at fixed $\langle n \rangle$, and this relationship can now be quantified: A linear fit to the data preceding the plateau gives a slope of −4.7 mV/equiv.

After observing opposing trends in E_F upon removal of e^-_{CB} or H^+, we questioned what net change would be observed upon removal of both as H atoms. Previous work has demonstrated spontaneous H atom transfer from these photodoped ZnO nanocrystals to the stable radical (2,2,6,6-tetramethylpiperidin-1-yl)oxyl ("TEMPO") to form the reduced hydroxyl amine TEMPOH.[21] Figure 1C plots the titration of ne^-,nH^+:ZnO nanocrystals using TEMPO (pathway C). With each added equivalent, V_{OC} steps positive with a linear slope of 12.1 mV/equiv until the data reach an inflection point, which again corresponds to $\langle n \rangle$. The ZnO nanocrystals are stabilized by 12.1 mV with the removal of each e^-_{CB}, but this effect is diminished compared to the trend observed in Figure 1A because of the concomitant deprotonation; as the titration progresses, the remaining e^-_{CB} are left with fewer charge-stabilizing H^+ than if an oxidant alone were used instead. On first glance, one might expect the slope resulting from titration by an H atom abstractor to equal the sum of the slopes derived from the oxidation and deprotonation titrations, i.e., +28.1 mV/equiv. The discrepancy between this expectation and experiment (+12.1 mV/equiv) is interpreted as primarily reflecting the fact that protonated "Proton Sponge" is still positively charged and hence can still stabilize the e^-_{CB} coulombically, albeit less effectively. The slope in Figure 1B is thus related to the free-energy change of replacing H^+ at the ZnO nanocrystal surface with protonated "Proton Sponge" ammonium cations. Complete removal of H^+ (or any charge-balancing cation) from n-doped ZnO nanocrystals is expected to yield a far more negative slope. Screening by the electrolyte may also diminish the experimental slope.

Potentiometric titrations have been a long-standing pillar of analytical chemistry,[22] yet we have found little precedent for titrations of samples involving so many electrons. Titrations have been performed with nanometer-sized Au clusters known to store a similar number of charges, but in that report the clusters were used as the titrant for measuring $E^{\circ\prime}$ of various analytes.[23] We propose that the linear slope shown in Figure 1A is inversely related to the capacitance of the ZnO nanocrystals. In the most general model, which is independent of classical and quantum mechanical effects, the capacitance is defined as given by eq 1. Here, the capacitance represents the change in charge (ΔQ) of a ZnO nanocrystal upon a change in potential (ΔV). From eq 1, the experimental slope in the data of Figure 1A indicates a capacitance of 4.9 ± 0.1 aF (attofarad) for these n-type d = 6.1 nm ZnO nanocrystals, with error determined from uncertainty in the linear fit of the data. This value is well within the range of capacitances simulated[24] and measured[25] for semiconductor nanocrystals, "ultramicroelectrodes",[26] and molecular thin films.[27−29]

$$\frac{1}{C} = \frac{1}{C_s A} \equiv \frac{\Delta V}{\Delta Q} \tag{1}$$

Equation 1 also shows that the capacitance can be described as the product of surface area (A) and a set of constants grouped together as the specific areal capacitance (C_s). This equation therefore predicts the linear slope ($\Delta V/\Delta Q$) to depend inversely on nanocrystal surface area, with larger nanocrystals exhibiting larger capacitance. Figure 2A plots potentiometric titrations for three sizes of ZnO nanocrystals, including the data from Figure 1A ([Fc*][BAr^F_4], pathway A). Indeed, the nanocrystals with d = 4.5 nm display the greatest $\Delta V/\Delta Q$, and hence the greatest capacitance, whereas those with d = 9.3 nm show the smallest $\Delta V/\Delta Q$ (see Table 1). The titration curves also exhibit striking similarities. Regardless of diameter, maximally photodoped ne^-,nH^+:ZnO nanocrystals all possess nearly identical V_{OC}. This observation confirms the same conclusion from our previous report, which used an optical redox indicator method for measuring E_F of photodoped ZnO nanocrystals of different sizes.[18]

From eq 1, the various slopes $\Delta V/\Delta Q$ shown in Figure 2A should all be related to a constant, C_S, times the nanocrystal surface area, A. Figure 2B replots the data from Figure 2A with the x-axis now recast as equivalents per nanocrystal surface area. In this representation, the data from all three nanocrystal sizes are essentially superimposable. The slight offsets in the V_{OC} drop are within the uncertainty of the nanocrystal size and concentration determination. Plotted in this manner, the data in Figure 2B yield a size-independent value of $C_S \approx 4\ \mu F\ cm^{-2}$. This value is remarkably similar to those reported for bulk metal-oxide semiconductors, determined using voltammetry or

DOI: 10.1021/jacs.6b05848
J. Am. Chem. Soc. 2016, 138, 10605−10610

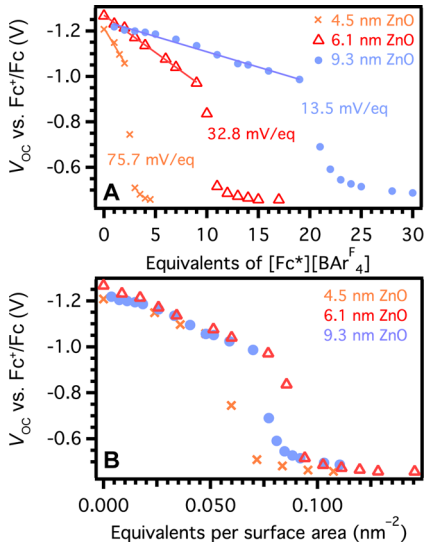

Figure 2. (A) Potentiometric titrations of d = 4.5, 6.1, and 9.3 nm colloidal ZnO nanocrystals using [Fc*][BAr^F_4] as the titrant. (B) Data from panel A, here with V_{OC} plotted vs charge equivalents per nanocrystal surface area. Crosses, open triangles, and closed circles correspond to d = 4.5, 6.1, and 9.3 nm ZnO nanocrystals, respectively.

Table 1. Comparison of Experimental Capacitance Values with Estimates from a Classical Double-Layer Model (eq 2) for the Colloidal ZnO Nanocrystals from Figure 2

ZnO nanocrystal diameter (nm)	experimental capacitance (aF)	C_{dl} (aF) from eq 2
4.5 ± 0.7	2.1 ± 0.2	3.6 ± 0.8
6.1 ± 1.0	4.9 ± 0.1	5.7 ± 1.5
9.3 ± 1.5	11.9 ± 0.4	11.1 ± 3.1

impedance spectroscopy on thin films.[30] Plotting the same data vs volumetric charge density does not lead to overlaying curves (Figure S5), even though the maximum electron density of *n*-type ZnO ($\langle N_{max} \rangle$) has been shown to depend on volume.[18] We conclude that the dependence of ΔV on ΔQ in colloidal ZnO nanocrystals is consistent with these nanocrystals behaving as simple capacitors.

DISCUSSION

Being neither small molecules nor bulk electrodes, it is unclear *a priori* whether the observed capacitance of colloidal ZnO nanocrystals originates from classical double-layer effects or from quantum mechanical effects. In molecules, there are few analogous systems capable of storing comparable charge density. These include fullerenes,[31−33] $Pt_n(CO)_m$ clusters,[34,35] thiolate-capped Au clusters,[23,36−40] and hexanuclear iron clusters.[41,42] Apart from the last example, the redox properties of these molecules have all been modeled in terms of classical double-layer capacitance (C_{dl}) assuming a metallic spherical electrode with an infinite density of states.[37,43] C_{dl} is defined as in eq 2 and is identical to that used for a classical electrostatic capacitor except with an additional term, t, to account for the thickness of the electrical double layer.[26,37] Here, A, ε_0, ε, and r refer to the sphere's surface area, the permittivity of free space, the dielectric constant of the solvent, and the nanocrystal radius, respectively. Consistent with this model, linear relationships have been found between the charge states of these systems and the corresponding formal potentials, $E^{\circ\prime}$.[43] Applying this classical model is counterintuitive, however, given that these systems are all molecules with a sparseness of discrete orbitals, which should make their multielectron redox transformations subject to orbital filling, spin-pairing, and other quantum effects. In fact, the orbital interactions in $Pt_{24}(CO)_{30}$[34] and 1 nm Au clusters[37,38] lead to distinctively uneven spacing between successive $E^{\circ\prime}$, but plots of $E^{\circ\prime}$ vs charge state are approximately linear.

$$C_{dl} = A\frac{\varepsilon_0\varepsilon}{r}\frac{r+t}{t} \tag{2}$$

Although simplistic, we explored the applicability of this classical double-layer model for analysis of the ZnO nanocrystal titration data. Surprisingly, eq 2 predicts capacitance values that are quite similar to what we measure experimentally. Assuming ε equal to the dielectric constant of bulk THF and a double-layer thickness of 2.5 nm, corresponding to the approximate length of an extended surface ligand plus a nearby TBA molecule, eq 2 predicts capacitances of 3.6 ± 0.8, 5.7 ± 1.5, and 11.1 ± 3.1 aF for the d = 4.5, 6.1, and 9.3 nm ZnO nanocrystals of Figure 2, respectively (see Table 1), with error determined by the uncertainty in nanocrystal size.

The accuracy of eq 2 is surprising, because the double-layer model does not account for the large orbital energy splittings and finite densities of states near the conduction-band edges of colloidal semiconductor nanocrystals. For example, the intra-conduction-band $1S_e$−$1P_e$ orbital energy gaps of the ZnO nanocrystals from Figure 2 are ∼0.25−0.35 eV, and the density of states is zero between these two orbitals in each nanocrystal. These nanocrystals should therefore be subject to quantum capacitance effects. The quantum capacitance, C_Q, is defined as shown in eq 3, where e is the elementary charge and $dQ/d\mu$ is the change in total charge per unit change in the chemical potential of the n electrons in the nanocrystal. According to eq 3, C_Q reflects the work required to place an additional e^- within a finite density of states centered at energy E, given by $g(E)$.[29,44,45] C_Q can also be defined in terms of ionization energy, electron affinity, and, hence, electronegativity.[45] Additional quantum Coulomb blockade effects are also anticipated in the low-electron limit.

$$C_Q = e\frac{dQ}{d\mu(n)} = e^2 g(E) \tag{3}$$

For nanometer-sized systems, the total capacitance (often called redox capacitance, C_r) is then described by C_{dl} in series with C_Q, as shown in eq 4.[44,46,47] Conceptually, eq 4 can be viewed as describing two concomitant energetic thresholds that electrons must surmount when transferring into the nanocrystal. Despite expectations from our spectroscopic understanding of these nanocrystals, the electrochemical titration data in Figure 2 show no evidence of quantum capacitance.

$$\frac{1}{C_r} = \frac{1}{C_{dl}} + \frac{1}{C_Q} \tag{4}$$

We propose that the experimental titration data appear entirely classical because these potentiometric titration measurements are performed on ensembles of nanocrystals. According to eqs 3 and 4, C_Q becomes evident when $g(E)$ is small, e.g., in an isolated nanocrystal or in a uniform ensemble with small densities of states between discrete orbitals. In real ensembles of ZnO nanocrystals, however, $g(E)$ is broadened by inhomogeneities in nanocrystal volume, countercation distri-

DOI: 10.1021/jacs.6b05848
J. Am. Chem. Soc. 2016, 138, 10605−10610

butions, surface-ligand coverages, faceting, and surface non-stoichiometries. As illustrated by the data in Figure 1 and by our previous observation that electrons in one-electron-reduced ZnO nanocrystals are more stable when charge-balanced by protons rather than $CoCp^*_2^+$,[18] relatively minor perturbations to the electrical double-layer can cause E_F for a given nanocrystal to vary by tens or even hundreds of mV, making double-layer heterogeneity arguably the major source of $g(E)$ broadening. The ensemble $g(E)$ thus does not vanish at any value of E, causing $1/C_Q$ to remain correspondingly small at all E. Consequently, the effects of quantized electronic structure are not discernible in the ensemble potentiometric titrations, and the experimental capacitance of the ZnO nanocrystal ensemble is instead dominated by the classical double-layer contributions. In this regard, electrochemistry diverges dramatically from the optical spectroscopies often used to characterize the electronic structures of colloidal semiconductor nanocrystals, which selectively measure *relative* inter- or intraband energies without sensitivity to inhomogeneities in *absolute* band-edge potentials.

In summary, potentiometric titrations have been used for contactless measurement of Fermi levels in colloidal *n*-type ZnO nanocrystals under equilibrium conditions across a broad range of carrier densities and nanocrystal volumes. Different titrants were demonstrated to lower or raise E_F by selectively removing e^-_{CB} or charge-balancing H^+. A linear relationship is found between E_F and $\langle n \rangle$, which can be used to quantify the capacitance of the ZnO nanocrystals. This interpretation is confirmed by the observation that the titration curves for nanocrystals of various diameters are essentially collinear once normalized for nanocrystal surface area. Although unexpected, the experimental results are described well using a classical, double-layer capacitance model. The dominance of classical double-layer capacitance reflects distributed band-edge potentials within the nanocrystal ensemble, in large part attributable to electrical double-layer heterogeneity and the strong dependence of the nanocrystal band-edge potentials on relatively small electrostatic or surface-dipole perturbations. Overall, these results and analysis provide new insights into the electronic properties of colloidal semiconductor nanocrystals relevant to their application as redox reagents, electronic device components, or photocatalysts.

More generally, potentiometric titration is an appealing methodology for tuning and measuring E_F of semiconductor nanocrystals that can store extra charge carriers, whether electrons or holes. The tunable carrier densities and absence of midgap electron traps in colloidal ZnO nanocrystals[48,49] make these nanocrystals ideal for demonstration of this technique, but extension of the methodology to more complex systems involving greater contributions from midgap traps, such as *n*-type CdSe, PbSe, TiO_2,[50] or meso-structured ZnO,[51] should also prove interesting.

■ ASSOCIATED CONTENT

Supporting Information

The Supporting Information is available free of charge on the ACS Publications website at DOI: 10.1021/jacs.6b05848.

Diagram of the experimental apparatus, balanced reaction equations, UV−vis−NIR spectra, additional titration data, and powder X-ray diffraction patterns (PDF)

■ AUTHOR INFORMATION

Corresponding Author

*gamelin@chem.washington.edu

Notes

The authors declare no competing financial interest.

■ ACKNOWLEDGMENTS

This research was supported by the NSF (CHE-1506014 to D.R.G., Graduate Research Fellowship DGE-1256082 to K.H.H.) and by the State of Washington through the University of Washington Clean Energy Institute via funding from the Washington Research Foundation (to C.K.B.). We are grateful to Prof. Bo Zhang for fruitful discussions.

■ REFERENCES

(1) Carey, G. H.; Abdelhady, A. L.; Ning, Z.; Thon, S. M.; Bakr, O. M.; Sargent, E. H. *Chem. Rev.* **2015**, *115*, 12732−12763.
(2) Mashford, B. S.; Stevenson, M.; Popovic, Z.; Hamilton, C.; Zhou, Z.; Breen, C.; Steckel, J.; Bulovic, V.; Bawendi, M.; Coe-Sullivan, S.; Kazlas, P. T. *Nat. Photonics* **2013**, *7*, 407−412.
(3) Talapin, D. V.; Lee, J. S.; Kovalenko, M. V.; Shevchenko, E. V. *Chem. Rev.* **2010**, *110*, 389−458.
(4) Simon, T.; Bouchonville, N.; Berr, M. J.; Vaneski, A.; Adrović, A.; Volbers, D.; Wyrwich, R.; Döblinger, M.; Susha, A. S.; Rogach, A. L.; Jäckel, F.; Stolarczyk, J. K.; Feldmann, J. *Nat. Mater.* **2014**, *13*, 1013−1018.
(5) Han, Z.; Qiu, F.; Eisenberg, R.; Holland, P. L.; Krauss, T. D. *Science* **2012**, *338*, 1321−1324.
(6) Kalisman, P.; Nakibli, Y.; Amirav, L. *Nano Lett.* **2016**, *16*, 1776−1781.
(7) Chen, C.; Shi, T.; Chang, W.; Zhao, J. *ChemCatChem* **2015**, *7*, 724−731.
(8) Brown, P. R.; Kim, D.; Lunt, R. R.; Zhao, N.; Bawendi, M. G.; Grossman, J. C.; Bulovic, V. *ACS Nano* **2014**, *8*, 5863−5872.
(9) Carroll, G. M.; Brozek, C. K.; Hartstein, K. H.; Tsui, E. Y.; Gamelin, D. R. *J. Am. Chem. Soc.* **2016**, *138*, 4310−4313.
(10) Germeau, A.; Roest, A. L.; Vanmaekelbergh, D.; Allan, G.; Delerue, C.; Meulenkamp, E. A. *Phys. Rev. Lett.* **2003**, *90*, 097401.
(11) Haase, M.; Weller, H.; Henglein, A. *J. Phys. Chem.* **1988**, *92*, 482−487.
(12) Liu, W. K.; Whitaker, K. M.; Kittilstved, K. R.; Gamelin, D. R. *J. Am. Chem. Soc.* **2006**, *128*, 3910−3911.
(13) Wood, A.; Giersig, M.; Mulvaney, P. *J. Phys. Chem. B* **2001**, *105*, 8810−8815.
(14) Schimpf, A. M.; Gunthardt, C. E.; Rinehart, J. D.; Mayer, J. M.; Gamelin, D. R. *J. Am. Chem. Soc.* **2013**, *135*, 16569−16577.
(15) Chávez, I.; Alvarez-Carena, A.; Molins, E.; Roig, A.; Maniukiewicz, W.; Arancibia, A.; Arancibia, V.; Brand, H.; Manuel Manríquez, J. *J. Organomet. Chem.* **2000**, *601*, 126−132.
(16) Norberg, N. S.; Gamelin, D. R. *J. Phys. Chem. B* **2005**, *109*, 20810−20816.
(17) Schwartz, D. A.; Norberg, N. S.; Nguyen, Q. P.; Parker, J. M.; Gamelin, D. R. *J. Am. Chem. Soc.* **2003**, *125*, 13205−13218.
(18) Carroll, G. M.; Schimpf, A. M.; Tsui, E. Y.; Gamelin, D. R. *J. Am. Chem. Soc.* **2015**, *137*, 11163−11169.
(19) Schwartz, D. A.; Gamelin, D. R. In *Proceedings of SPIE-The International Society for Optical Engineering*; Cao, G., Xia, Y., Braun, P. V., Eds.; 2003; Vol. *5224*, p 1.
(20) Pesika, N. S.; Stebe, K. J.; Searson, P. C. *Adv. Mater.* **2003**, *15*, 1289−1291.
(21) Schrauben, J. N.; Hayoun, R.; Valdez, C. N.; Braten, M.; Fridley, L.; Mayer, J. M. *Science* **2012**, *336*, 1298−1301.
(22) Kolthoff, I. M.; Furman, N. H. *Potentiometric titrations, a theoretical and practical treatise*, 2nd ed.; J. Wiley & Sons: 1931.
(23) Pietron, J. J.; Hicks, J. F.; Murray, R. W. *J. Am. Chem. Soc.* **1999**, *121*, 5565−5570.

DOI: 10.1021/jacs.6b05848
J. Am. Chem. Soc. 2016, 138, 10605−10610

(24) Macucci, M.; Hess, K.; Iafrate, G. J. *J. Appl. Phys.* **1995**, *77*, 3267−3276.
(25) Chan, I. H.; Westervelt, R. M.; Maranowski, K. D.; Gossard, A. C. *Appl. Phys. Lett.* **2002**, *80*, 1818−1820.
(26) Wang, H.; Pilon, L. *J. Phys. Chem. C* **2011**, *115*, 16711−16719.
(27) Bueno, P. R.; Mizzon, G.; Davis, J. J. *J. Phys. Chem. B* **2012**, *116*, 8822−8829.
(28) Bueno, P. R.; Davis, J. J. *Anal. Chem.* **2014**, *86*, 1997−2004.
(29) Bueno, P. R.; Davis, J. J. *Anal. Chem.* **2014**, *86*, 1337−1341.
(30) Munoz, A. G. *Photoelectrochemical Solar Conversion Systems*, 1st ed.; CRC Press: Boca Raton, 2013.
(31) Dubois, D.; Kadish, K. M.; Flanagan, S.; Haufler, R. E.; Chibante, L. P. F.; Wilson, L. J. *J. Am. Chem. Soc.* **1991**, *113*, 4364−4366.
(32) Dubois, D.; Kadish, K. M.; Flanagan, S.; Wilson, L. J. *J. Am. Chem. Soc.* **1991**, *113*, 7773−7774.
(33) Li, Q.; Wudl, F.; Thilgen, C.; Whetten, R. L.; Diederich, F. *J. Am. Chem. Soc.* **1992**, *114*, 3994−3996.
(34) Lewis, G. J.; Roth, J. D.; Montag, R. A.; Safford, L. K.; Gao, X.; Chang, S. C.; Dahl, L. F.; Weaver, M. J. *J. Am. Chem. Soc.* **1990**, *112*, 2831−2832.
(35) Roth, J. D.; Lewis, G. J.; Safford, L. K.; Jiang, X.; Dahl, L. F.; Weaver, M. J. *J. Am. Chem. Soc.* **1992**, *114*, 6159−6169.
(36) Ingram, R. S.; Hostetler, M. J.; Murray, R. W.; Schaaff, T. G.; Khoury, J. T.; Whetten, R. L.; Bigioni, T. P.; Guthrie, D. K.; First, P. N. *J. Am. Chem. Soc.* **1997**, *119*, 9279−9280.
(37) Chen, S.; Murray, R. W.; Feldberg, S. W. *J. Phys. Chem. B* **1998**, *102*, 9898−9907.
(38) Chen, S.; Ingram, R. S.; Hostetler, M. J.; Pietron, J. J.; Murray, R. W.; Schaaff, G.; Khoury, J. T.; Alvarez, M. M.; Whetten, R. L. *Science* **1998**, *280*, 2098−2101.
(39) Hicks, J. F.; Miles, D. T.; Murray, R. W. *J. Am. Chem. Soc.* **2002**, *124*, 13322−13328.
(40) Quinn, B. M.; Liljeroth, P.; Ruiz, V.; Laaksonen, T.; Kontturi, K. *J. Am. Chem. Soc.* **2003**, *125*, 6644−6645.
(41) Hernández Sánchez, R.; Zheng, S.-L.; Betley, T. A. *J. Am. Chem. Soc.* **2015**, *137*, 11126−11143.
(42) Zhao, Q.; Harris, T. D.; Betley, T. A. *J. Am. Chem. Soc.* **2011**, *133*, 8293−8306.
(43) Weaver, M. J.; Gao, X. *J. Phys. Chem.* **1993**, *97*, 332−338.
(44) Büttiker, M.; Thomas, H.; Prêtre, A. *Phys. Lett. A* **1993**, *180*, 364−369.
(45) Iafrate, G. J.; Hess, K.; Krieger, J. B.; Macucci, M. *Phys. Rev. B: Condens. Matter Mater. Phys.* **1995**, *52*, 10737−10739.
(46) Bueno, P. R.; Feliciano, G. T.; Davis, J. J. *Phys. Chem. Chem. Phys.* **2015**, *17*, 9375−9382.
(47) Luryi, S. *Appl. Phys. Lett.* **1988**, *52*, 501−503.
(48) Schimpf, A. M.; Ochsenbein, S. T.; Buonsanti, R.; Milliron, D. J.; Gamelin, D. R. *Chem. Commun.* **2012**, *48*, 9352−9354.
(49) Hayoun, R.; Whitaker, K. M.; Gamelin, D. R.; Mayer, J. M. *J. Am. Chem. Soc.* **2011**, *133*, 4228−4231.
(50) Szczepankiewicz, S. H.; Moss, J. A.; Hoffmann, M. R. *J. Phys. Chem. B* **2002**, *106*, 7654−7658.
(51) Parthasarathy, M.; Ramgir, N. S.; Sathe, B. R.; Mulla, I. S.; Pillai, V. K. *J. Phys. Chem. C* **2007**, *111*, 13092−13102.

DOI: 10.1021/jacs.6b05848
J. Am. Chem. Soc. 2016, 138, 10605−10610